www.czasopisma.pan.pl PAN www.journals.pan.pl
POLSKA AKADEMIA NAUK

10.24425/acs.2019.131229

Archives of Control Sciences
Volume 29(LXV), 2019
No. 4, *pages 617–642*

Synchronization of neuronal bursting using backstepping control with recursive feedback

SURESH RASAPPAN

J.L. Hindmarsh, R.M. Rose introduced the concept of neuronal burst. In this paper, synchronization is investigated for the construction of a model of neuronal burst using backstepping control with recursive feedback. Synchronization for a model of neuronal bursting system is established using Lyapunov stability theory. The backstepping scheme is a recursive procedure that links the choice of a Lyapunov function with the design of a controller. The backstepping control method is effective and convenient to synchronize identical systems. Numerical simulations are furnished to illustrate and validate the synchronization result derived in this paper.

Key words: Hindmarsh-Rose neuronal bursting system, chaos, synchronization, backstepping control, Lyapunov, stability

1. Introduction

Chaotic systems are highly sensitive depending on their initial conditions. The synchronization of two or more systems is not easy to achieve [1–3], as the sensitive initial conditions and time delay are the factors that affect the synchronization [4–6].

The most striking aspect of a chaos synchronization is that it can share a common dynamical behaviour under the background. Synchronization has potential application in various fields such as secure communication [7, 8], physical systems [9], chemical reaction [10], ecological systems [11], information science [12], energy resource systems [13], ghost burster neurons [14], bi-axial magnet models [15], neuronal models [16, 17], IR epidemic models with impulsive vaccination [18], predicting the influence of solar wind to celestial bodies [19], etc., [20–38].

Recently, chaos theory has been applied in the field of biomedicine to explain the cardiac and neural tissue to pacing stimuli, therapeutic intervention, neuronal

S. Rasappan is with Department of Mathematics, Vel Tech University, 400 Feet Outer Ring Road, Avadi, Tamil Nadu, Chennai-600 062, India. E-mail: mrpsuresh83@gmail.com

Received 02.04.2019. Revised 10.11.2019.

systems, etc., [39–42]. Due to the fact that the brain acts as the intricate part of the human body, chaos theory and dynamical equations provide a good base for studying it. In the model of electrical signals of nerves in the brain, chaos theory can help in the field of neurological diseases and also to the achievement of the invention of artificial intelligence [43–46].

In recent years, a backstepping method has been developed for designing controllers to control the chaotic systems [47]. A generally followed concept of the method is the design of a globally stable control chaotic system. The backstepping method is based on the mathematical model of the examined system, wherein new variables are introduced in a form depending on the state variables, controlling parameters and stabilizing functions. The difficult task of stabilizing a chaotic system is to remove nonlinearities from the system that influence the stability of its operation. The use of backstepping method comes in handy to create an additional non-linearity and eliminates the undesirable nonlinearities from the system.

The purpose of this paper is to propose a backstepping control design with novel feedback input approach. Our concept is a systematic design approach that guarantees global stability of the chaotic systems. Based on the Lyapunov function, the backstepping control is determined to tune the controller gain based on the precalculated feedback control inputs.

This paper is organized as follows. Section 2, present the methodology of chaos synchronization by backstepping control method. Section 3, provide a description of the chaotic systems discussed in this paper. Section 4 is devoted to the demonstration of the synchronization of identical neuronal bursting system [48, 49]. The results of the study are summarized in Section 5.

2. The problem statement and methodology

In general, two coupled dynamic systems in a synchronization scheme are called the master and slave systems, respectively. A well designed controller will make the trajectory of the slave system to track the trajectory of the master system, that is, the two systems will be synchronous.

Consider the chaotic system described by the dynamics

$$
\begin{aligned}
\dot{x}_1 &= F_1(x_1, x_2, \ldots, x_n),\\
\dot{x}_2 &= F_2(x_1, x_2, \ldots, x_n),\\
\dot{x}_3 &= F_3(x_1, x_2, \ldots, x_n),\\
\vdots\ \ &\ \vdots \qquad \vdots\\
\dot{x}_n &= F_n(x_1, x_2, \ldots, x_n),
\end{aligned}
\tag{1}
$$

where $x(t) \in R^n$ is a state of the system. The system (1) is considered as master system. Also the chaotic system described by the dynamics with the controller u as

$$\begin{aligned} \dot{y_1} &= G_1(y_1, y_2, \ldots, y_n) + u_1(t), \\ \dot{y_2} &= G_2(y_1, y_2, \ldots, y_n) + u_2(t), \\ \dot{y_3} &= G_3(y_1, y_2, \ldots, y_n) + u_3(t), \\ &\vdots \quad \vdots \qquad \vdots \\ \dot{y_n} &= G_n(y_1, y_2, \ldots, y_n) + u_n(t) \end{aligned} \tag{2}$$

is considered the slave system, where $y(t) \in R^n$ is a state of the system and F_i, G_i $(i = 1, 2, 3, \ldots, n)$ are linear and nonlinear functions with inputs from systems (1) and (2). If F_i equals to G_i, then the systems states are identical otherwise that systems states are non identical. The chaotic systems (1) and (2) depend not only on state variables but also on time t.

The synchronization error is defined as $e_i = y_i - x_i$; $i = 1, 2, 3, \ldots, n$, then the synchronization error dynamics is obtained as

$$\begin{aligned} \dot{e_1} &= G_1(y_1, y_2, \ldots, y_n) - F_1(x_1, x_2, \ldots, x_n) + u_1(t), \\ \dot{e_2} &= G_2(y_1, y_2, \ldots, y_n) - F_2(x_1, x_2, \ldots, x_n) + u_2(t), \\ \dot{e_3} &= G_3(y_1, y_2, \ldots, y_n) - F_3(x_1, x_2, \ldots, x_n) + u_3(t), \\ &\vdots \quad \vdots \qquad \vdots \\ \dot{e_n} &= G_n(y_1, y_2, \ldots, y_n) - F_4(x_1, x_2, \ldots, x_n) + u_n(t). \end{aligned} \tag{3}$$

The synchronization error system controls a controlled chaotic system with control input u_i, $i = 1, 2, 3, \ldots, n$ as a function of the error states $e_1, e_2, e_3, \ldots, e_n$. That means the systematic feedbacks so as to stabilize the error dynamics (3), e_1, $e_2, e_3, \ldots, e_n$ converge to zero as time $t \to \infty$. This implies that the controllers u_i, $i = 1, 2, 3, \ldots, n$ should be designed so that the two chaotic systems can be synchronized. In mathematical,

$$\lim_{t\to\infty} \|e(t)\| = 0.$$

Backstepping design is recursive and guarantees global stabilities performance of strict-feedback chaotic systems. By using the backstepping design, at the i^{th} step, the i^{th} order subsystem is stabilized with respect to a Lyapunov function V_i by the design of virtual control α_i and a control input function u_i.

We consider the stability of the system,

$$\dot{e_1} = G_1(y_1, y_2, \ldots, y_n) - F_1(x_1, x_2, \ldots, x_n) + u_1(t), \tag{4}$$

where u_1 is control input, which is the function of the error state vectors e_i, and the state variables $x(t) \in R^n$, $y(t) \in R^n$. As long as this feedback stabilizes the system (4) converges to zero as the time $t \to \infty$, where $e_2 = \alpha_1(e_1)$ is regarded as virtual controller.

For the design of $\alpha_1(e_1)$ to stabilize the subsystem (4), we consider the Lyapunov function defined by

$$V_1(e_1) = e_1^T P_1 e_1 , \tag{5}$$

where P_1 is is a positive definite matrix. The derivative of V_1 is

$$\dot{V}_1 = -e_1^T Q_1 e_1 , \tag{6}$$

where Q_1 is a positive definite matrix, then $\dot{V}_1$ is a negative definite function on R^n. Thus by Lyapunov stability theory [50] the error dynamics (4) is asymptotically stable. The virtual control $e_2 = \alpha_1(e_1)$ and the state feedback input u_1 makes the system (4) asymptotically stable. The function $\alpha_1(e_1)$ is estimative when e_2 is considered as controller.

The error between e_2 and $\alpha_1(e_1)$ is

$$w_2 = e_2 - \alpha_1(e_1). \tag{7}$$

Considering the (e_1, w_2) subsystem given by

$$\begin{aligned} \dot{e}_1 &= G_1(y_1, y_2, \dots, y_n) - F_1(x_1, x_2, \dots, x_n) + u_1 , \\ \dot{w}_2 &= G_2(y_1, y_2, \dots, y_n) - F_2(x_1, x_2, \dots, x_n) - \dot{\alpha}_1(e_1) + u_2 . \end{aligned} \tag{8}$$

Consider e_3 as a virtual controller in system (8), assume when it is equal to $\alpha_2(e_1, w_2)$ and it makes system (8) asymptotically stable. Consider the Lyapunov function defined by

$$V_2(e_1, w_2) = V_1(e_1) + w_2^T P_2 w_2 , \tag{9}$$

where P_2 is is a positive definite matrix. The derivative of V_2 is

$$\dot{V}_2 = e_1^T Q_1 e_1 , \tag{10}$$

where Q_1, Q_2 are positive definite matrices, then $\dot{V}_2$ is a negative definite function on R^n. Thus by Lyapunov stability theory the error dynamics (8) is asymptotically stable. The virtual control $e_2 = \alpha_2(e_1, w_2)$ and the state feedback input u_2 makes the system (8) asymptotically stable. For the n^{th} state of the error dynamics, define the error variable w_n as

$$w_n = e_n - \alpha_{n-1}(e_1, w_2, w_3, \dots, w_n). \tag{11}$$

Considering the $(e_1, w_2, w_3, \dots, w_n)$ subsystem given by

$$\begin{aligned} \dot{e}_1 &= G_1(y_1, y_2, \dots, y_n) - F_1(x_1, x_2, \dots, x_n) + u_1 , \\ \dot{w}_2 &= G_2(y_1, y_2, \dots, y_n) - F_1(x_1, x_2, \dots, x_n) - \alpha_1(e_1) + u_2 , \\ \dot{w}_n &= G_n(y_1, y_2, \dots, y_n) - F_1(x_1, x_2, \dots, x_n) \\ &\quad - \alpha_{n-1}(e_1, w_2, w_3, \dots, w_n) + u_n . \end{aligned} \tag{12}$$

Consider the Lyapunov function defined by

$$V_n(e_1, w_2, w_3, \ldots, w_n) = V_{n-1}(e_1, w_2, w_3, \ldots, w_{n-1}) + w_n^T P_n w_n, \tag{13}$$

where P_n is a positive definite matrix. The derivative of V_n is

$$\dot{V}_n = -e_1^T Q_1 e_1 - w_2^T Q_2 w_2 - \ldots - w_n^T Q_n w_n, , \tag{14}$$

where Q_1, Q_2, Q_3, $\ldots$, Q_n are positive definite matrices, then $\dot{V}_n$ is a negative definite function on R^n. Thus by Lyapunov stability theory the error dynamics (12) is asymptotically stable. The virtual control $e_n = \alpha_{n-1}(e_1, w_2, w_3, \ldots, w_{n-1})$ and the state feedback input u_n makes the system (12) asymptotically stable. Thus by Lyapunov stability theory [50], the error dynamics (3) is globally exponentially stable and satisfied for all initial conditions $e(0) \in R^n$. Hence, the states of the master and slave systems are globally and exponentially synchronized.

3. System description

A model of nerve impulse system is based on Fitzhugh equation. The generalization of this model assumes that the rate of change of membrane potential (x_1) depends linearly on the current passing through the electrode (x_2) and an intrinsic current (x_3) depending nonlinearly on membrane potential [48, 49].

The membrane potential is given by

$$\dot{x}_1 = x_2 - f(x_1), \tag{15}$$

where $f(x_1)$ is governed by the relation

$$f(x) = ax_1^3 - bx_1^2$$

and the rate of intrinsic current is provided by

$$\dot{x}_2 = g(x_1) - x_2, \tag{16}$$

where $g(x)$ is furnished by

$$g(x) = c - dx_1^2.$$

The difference between the two concerned systems is that the Hindrose equation is parabolic in contrast to the form of straight line assumed by the Fitzhugh equation.

To stimulate the neuronal system, an intracellular recording from a small identified cell in the vis-ceral ganglion of the pond snail Lymnaea is introduced. Usually Lymnaea is silent. However, when it is depolarized, it fires several times and continues to fire after cessation of the stimulating current. Now the external current I is added into the membrane potential. The modified two-dimensional Hindmarsh-Rose system is given by [48, 49].

$$\begin{aligned} \dot{x}_1 &= x_2 - ax_1^3 + bx_1^2 + I, \\ \dot{x}_2 &= c - dx_1^2 - x_2 \,. \end{aligned} \tag{17}$$

The difference between neuronal burst and the cell is always necessary to fire the cell several times during the application of the current pulse for an after-discharge to occur. During the short current pulse, the fire is produced after discharge. Inward current is slower activation kinetic in the snail Lymnaea. Greater undershoot and rapid recovery are possible in recorded action potentials. The cell in Lymnaea, does not fire indefinitely, but slows down and is terminated with a slow after hyperpolarizing wave. By the introduction of a slow current, the Lymnaea cells are gradually hyperpolarized. A slowly increasing outward current has been reported to cause adaption in molluscan neurons which is generally underlies the depolarization process in molluscan bursters. Let r denote the ratio of slow current and fast current in Lymnaea.

The mathematical expression of an adaption current x_3 is given by [48, 49]

$$\dot{x}_3 = r(s(x_1 - x_0) - x_3). \tag{18}$$

The Hindmarsh-Rose neuronal bursting system is given [48, 49]

$$\begin{aligned} \dot{x}_1 &= x_2 - ax_1^3 + bx_1^2 + I, \\ \dot{x}_2 &= c - dx_1^2 - x_2 \,, \\ \dot{x}_3 &= r(s(x_1 - x_0) - x_3). \end{aligned} \tag{19}$$

where x_1 describes the membrane potential, x_2 describes the exchange of ions across the neuron membrane through fast ionic channels and x_3 the change of ions through slow ionic channels.

The parameters a, b, c, d are constants determined experimentally and $x_0 = -\frac{1}{2}(1+\sqrt{5})$ is the equilibrium $x-$ coordinate of system (19) for the parameters

$$a = 1, \quad b = 3, \quad c = 1, \quad d = 5, \quad r \leqslant 1, \quad \text{and} \quad s = 4. \tag{20}$$

It take up the question of occurrence of different types of a bursting cell. The system of differential equations can be modeled as a bursting cell when the current parameter I is set at a constant level.

Let us consider r as a variable, while the value of I is fixed. With the choice of the parameters $I = 3.25$, $a = 1$, $b = 3$, $c = 1$, $d = 5$, and $s = 4$, the model generates a classical period doubling cascade. Fig. 1 and Fig. 2 illustrating the

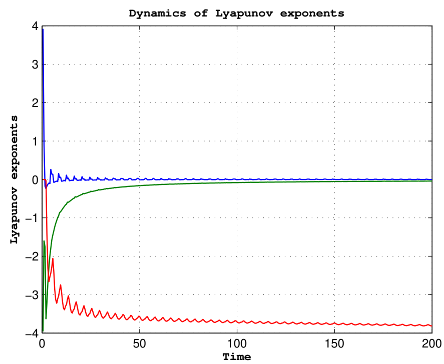

a) Lyapunov exponents $L_1 = -0.001829$, $L_2 = -0.042157$, $L_3 = -3.815855$ of (19) with parameters given in (20) and $I = 3.25$, $r = 0.00041$

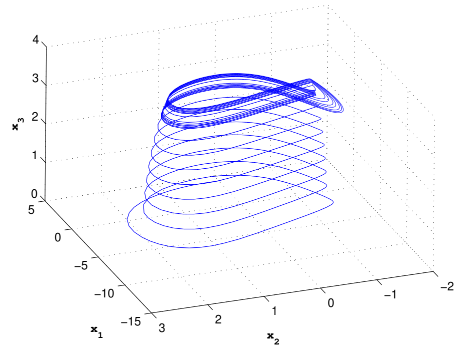

b) $(x,\ y,\ z)$ phase portraits of the system (19) with parameters given in (20) and with $I = 3.25$ for $r = 0.0145$

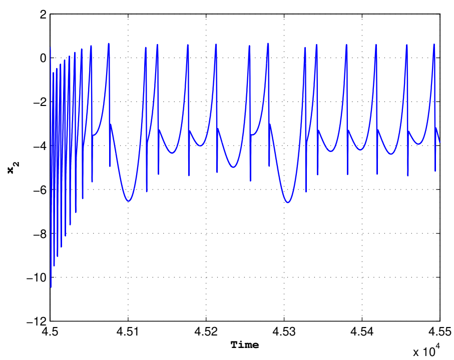

c) Time series portraits of the system (19) with parameters given in (20) and with $I = 3.25$ for $r = 0.0.0145$, a period doubling cascade is observed

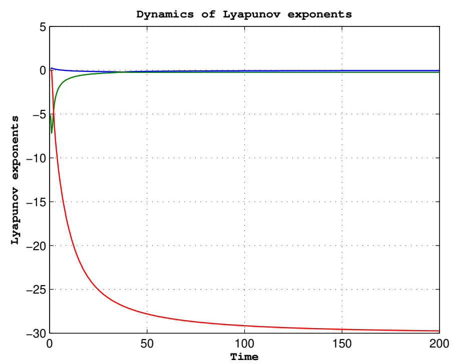

d) Lyapunov exponents $L_1 = -0.032696$, $L_2 = -0.226844$, $L_3 = -29.730009$ of (19) with parameters given in (20) and $I = 3.25$, $r = 0.0001$

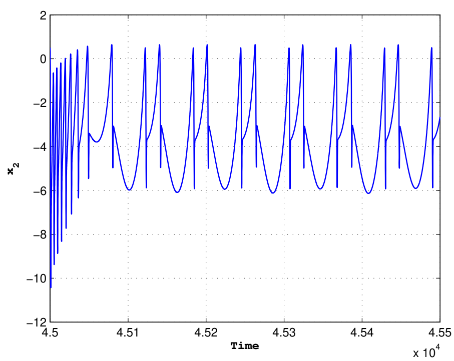

e) $(x,\ y,\ z)$ phase portraits of the system (19) with parameters given in (20) and with $I = 3.25$ for $r = 0.017$

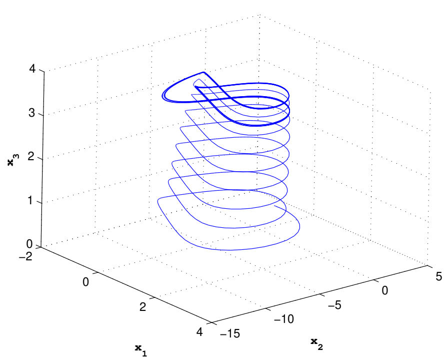

f) Time series portraits of the system (19) with parameters given in (20) and with $I = 3.25$ for $r = 0.017$, a period doubling cascade is observed

Figure 1: Phase portraits of bursting bifurcation phenomena

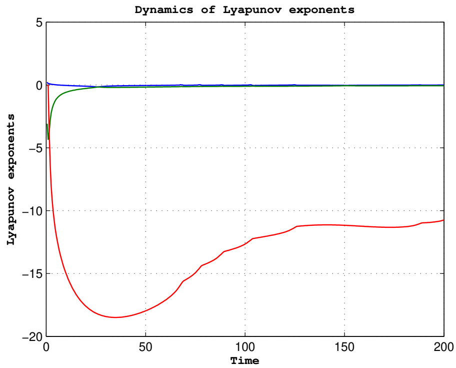

a) Lyapunov exponents $L_1 = -0.002382$, $L_2 = -0.059071$, $L_3 = -10.738918$ of (19) with parameters given in (20) and $I = 3.25$, $r = 0.008$

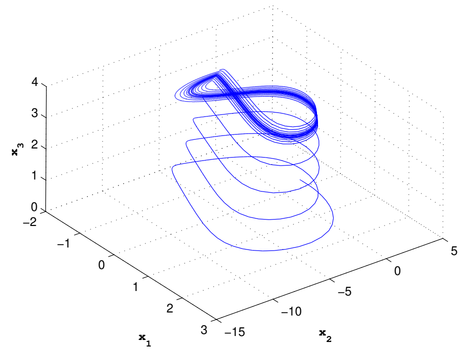

b) $(x,\ y,\ z)$ phase portraits of the system (19) with parameters given in (20) and with $I = 3.25$ for $r = 0.03$

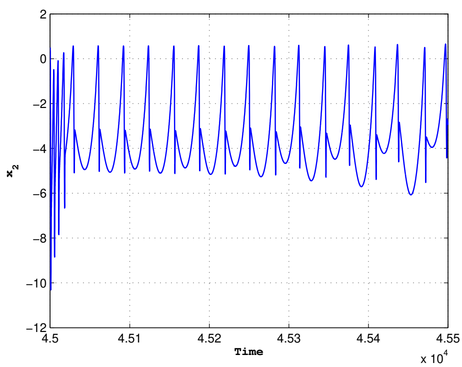

c) Time series portraits of the system (19) with parameters given in (20) and with $I = 3.25$ for $r = 0.0.03$, a period doubling cascade is observed

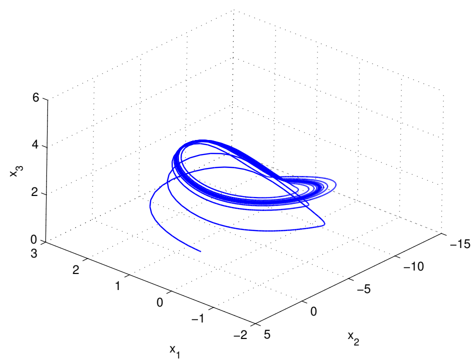

d) $(x,\ y,\ z)$ phase portraits of the system (19) with parameters given in (20) and with $I = 3.25$ for $r = 0.05$

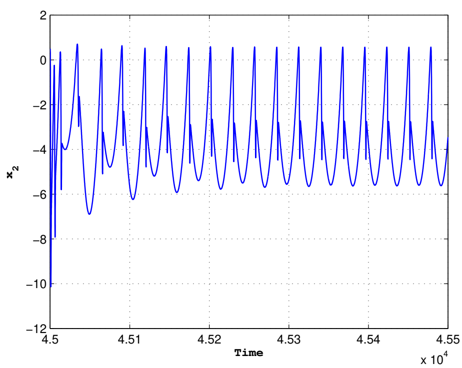

e) Time series portraits of the system (19) with parameters given in (20) and with $I = 3.25$ for $r = 0.05$, a period doubling cascade is observed

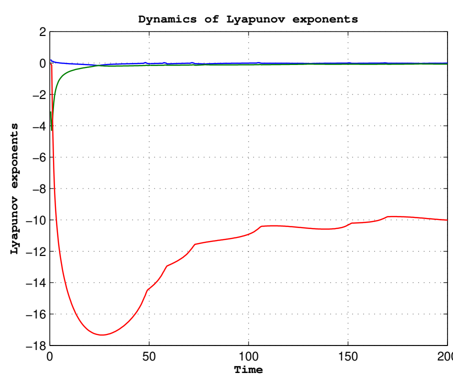

f) Lyapunov exponents $L_1 = -0.011976$, $L_2 = -0.0065696$, $L_3 = -10.010001$ of (19) with parameters given in (20) and $I = 3.25$, $r = 0.0145$

Figure 2: Phase portraits of bursting bifurcation phenomena

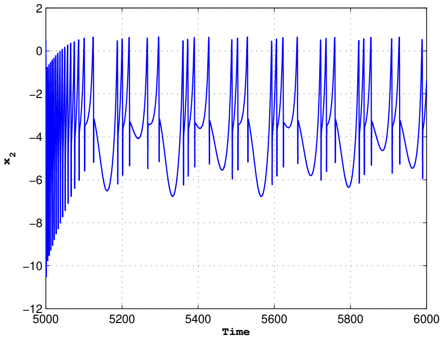

a) Time series portraits of the system (19) with parameters given in (20) and with $I = 3.25$ for $r = 0.008$, a period doubling cascade with a period three solution is observed

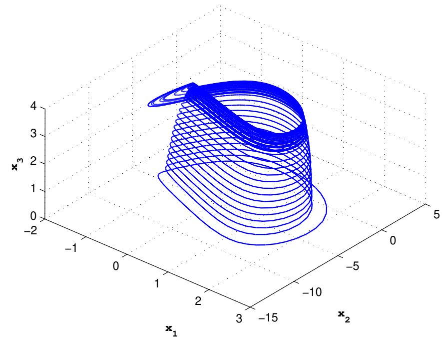

b) $(x,\ y,\ z)$ phase portraits of the system (19) with parameters given in (20) and with $I = 3.25$ for $r = 0.008$

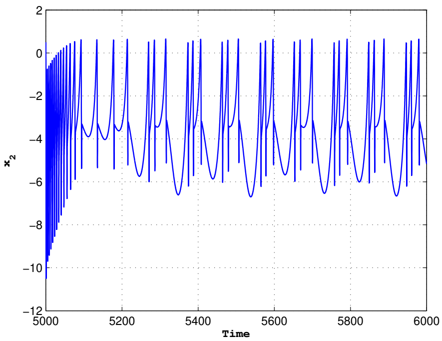

c) Time series portraits of the system (19) with parameters given in (20) and with $I = 3.25$ for $r = 0.0095$, a period doubling cascade with a period three solution is observed

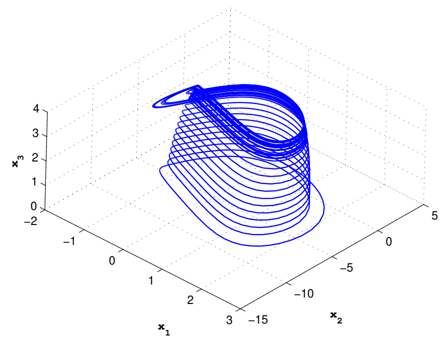

d) $(x,\ y,\ z)$ phase portraits of the system (19) with parameters given in (20) and with $I = 3.25$ for $r = 0.0095$

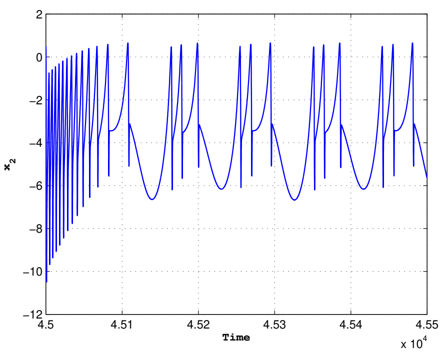

e) Time series portraits of the system (19) with parameters given in (20) and with $I = 3.25$ for $r = 0.01$, a period doubling cascade with a period three solution is observed

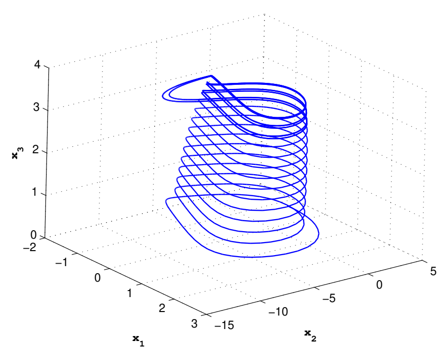

f) $(x,\ y,\ z)$ phase portraits of the system (19) with parameters given in (20) and with $I = 3.25$ for $r = 0.01$

Figure 3: Phase portraits of period doubling cascade starting with a period three solution

www.czasopisma.pan.pl www.journals.pan.pl

bursting bifurcation phenomena in the HR model with parameters given in (20) and $I = 3.25$. As this slow parameter increases, the period which corresponds to the number of spikes per burst decreases. A classical period doubling cascade is observed.

Fig. 3 illustrates the bursting bifurcation phenomena in the HR model (19) with parameters given by (20) and $I = 3.25$. We observe a period doubling cascade starting with a solution of period three.

Fig. 4 illustrates the bursting bifurcation phenomena in the HR model (19) with parameters given by (20) and $I = 3.25$. According to the chosen parameter r, the neuron behaviour changes from tonic to spiking to bursting.

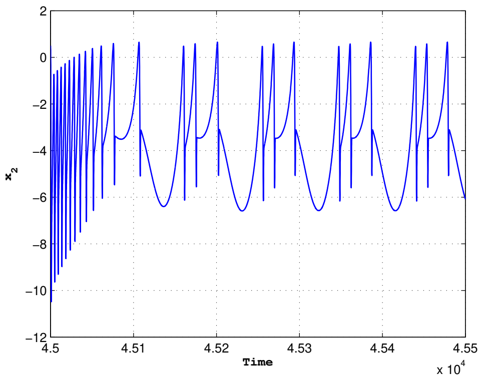

a) Time series portraits of the system (19) with parameters given in (20) and with $I = 3.25$ for $r = 0.011$, a period doubling case cade with a period three solution is observed

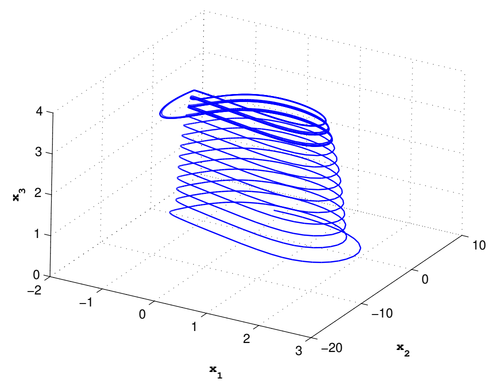

b) $(x,\ y,\ z)$ phase portraits of the system (19) with parameters given in (20) and with $I = 3.25$ for $r = 0.011$

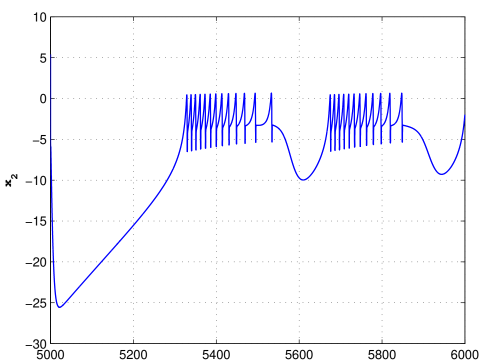

c) Time series portraits of the system (19) with parameters given in (20) and with $I = 3.25$ for $r = 0.002$, the neuron behavior changes from tonic spiking to bursting is observed

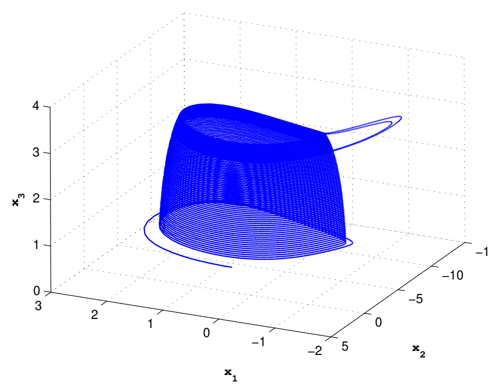

d) $(x,\ y,\ z)$ phase portraits of the system (19) with parameters given in (20) and with $I = 3.25$ for $r = 0.002$

Figure 4: Phase portraits of the neuron behavior changes from tonic spiking to bursting

Fig. 4 and Fig. 5 illustrate the model (19) with parameters given by (20) for the choosen values of parameters I. Moreover, for each value of I, there is the same number of spikes within burst in time series and same number of laps in the phase portraits.

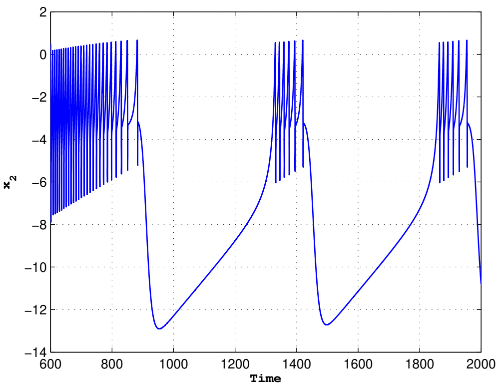

a) Time series portraits of the system (19) with parameters given in (20) with $I = 1.5$ for $r = 0.001$, a period doubling cascade with a period three solution is observed

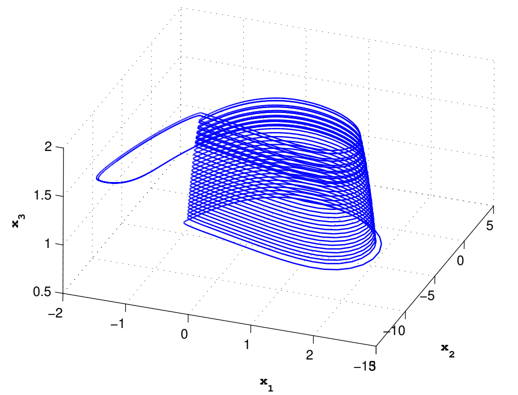

b) $(x,\ y,\ z)$ phase portraits of the system (19) with parameters given in (20) with $I = 1.5$ for $r = 0.001$

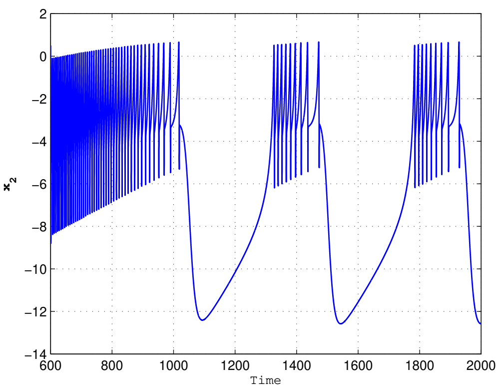

c) Time series portraits of the system (19) with parameters given in (20) with $I = 2$ for $r = 0.001$, the neuron behaviour changes from tonic spiking to bursting is observed

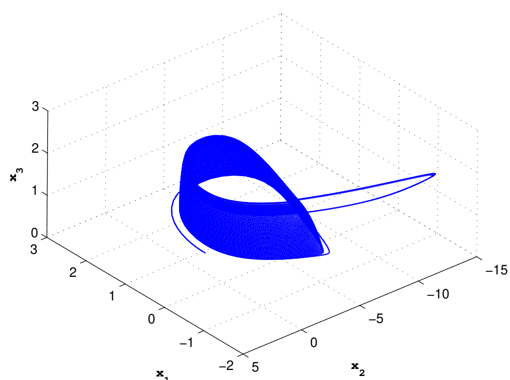

d) $(x,\ y,\ z)$ phase portraits of the system (19) with parameters given in (20) with $I = 2$ for $r = 0.001$

Figure 5: Phase portraits illustrating show a periodic behavior of system (19) for the chosen values of parameter I and spikes and laps

With the choice of parameters as $I = 0.4$, $a = 1$, $b = 3$, $c = 1$, $d = 5$, $r = 0.005$, and $s = 4$, the model generates an isolated burst followed by an after hyperpolarizing wave. Fig. 6 illustrate an isolated burst followed by an after hyperpolarizing wave.

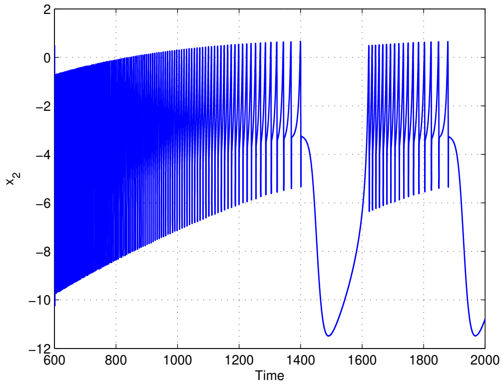

a) Time series portraits of the system (19) with parameters given in (20) with $I = 3$ for $r = 0.001$, a period doubling cascade with a period three solution is observed

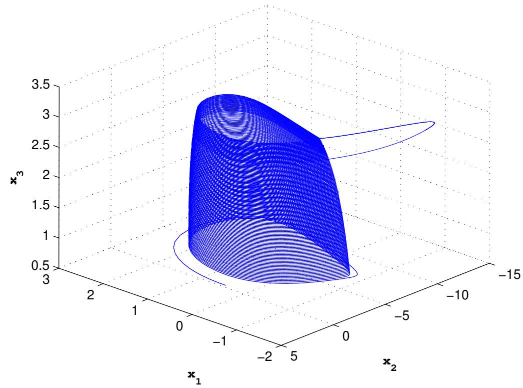

b) (x, y, z) phase portraits of the system (19) with parameters given in (20) with $I = 3$ for $r = 0.001$

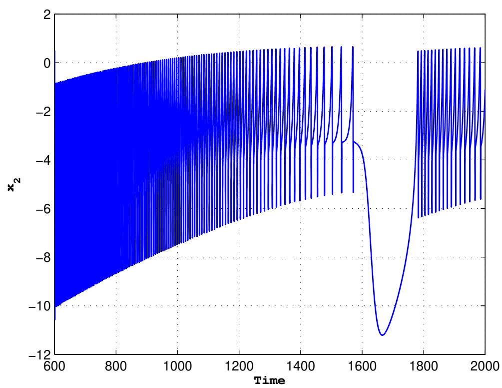

c) Time series portraits of the system (19) with parameters given in (20) with $I = 3.25$ for $r = 0.001$, the neuron behaviour changes from tonic spiking to bursting is observed

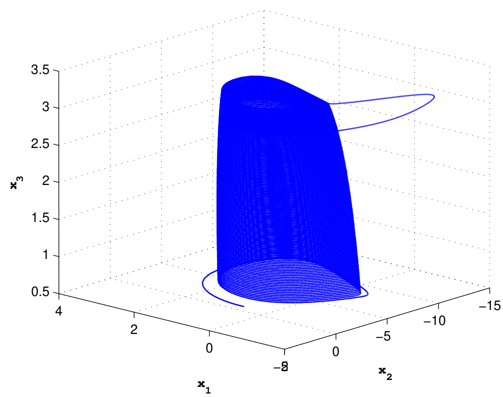

d) (x, y, z) phase portraits of the system (19) with parameters given in (20) with $I = 3.25$ for $r = 0.001$

Figure 6: Phase portraits illustrating show a periodic behavior of system (19) for the chosen values of parameter I and spikes and laps

When $I = 2$, $a = 1$, $b = 3$, $c = 1$, $d = 5$, $r = 0.005$, and $s = 4$, the model has a long burst initially in response to the current step and terminates to give the periodic burst pattern. Fig. 7 illustrates the periodic burst pattern.

When $I = 4$, $a = 1$, $b = 3$, $c = 1$, $d = 5$, $r = 0.005$, and $s = 4$. The model has a continuous high frequency discharge, with the frequency declining from

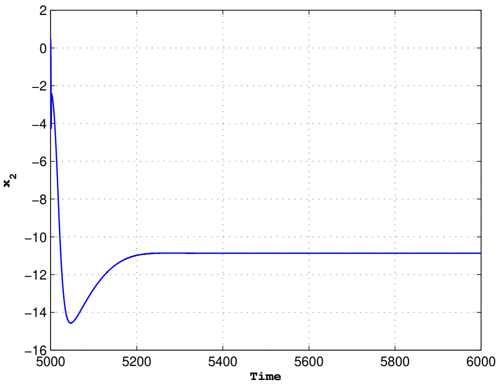

a) Time series portraits of the system (19) with parameters given in (20) with $I = 3$ for $r = 0.001$, a period doubling cascade with a period three solution is observed

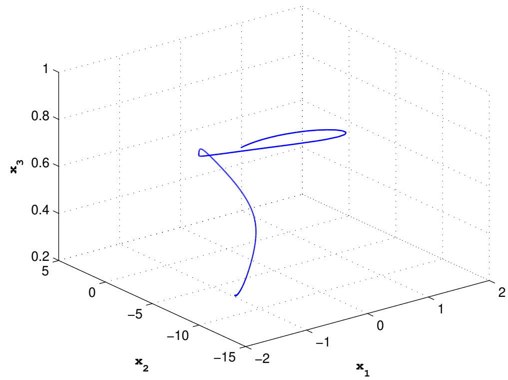

b) $(x,\ y,\ z)$ phase portraits of the system (19) with parameters given in (20) with $I = 3$ for $r = 0.001$

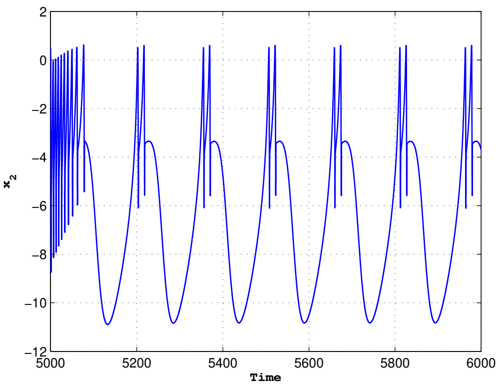

c) Time series portraits of the system (19) with parameters given in (20) with $I = 3.25$ for $r = 0.001$, the neuron behaviour changes from tonic spiking to bursting is observed

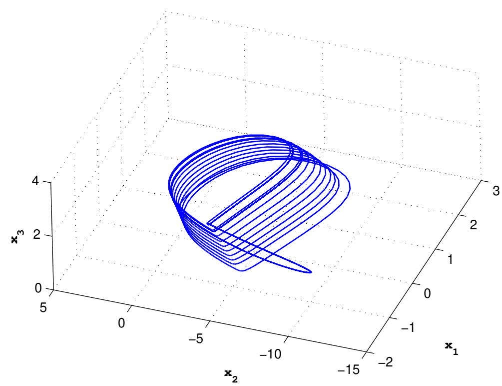

d) $(x,\ y,\ z)$ phase portraits of the system (19) with parameters given in (20) with $I = 3.25$ for $r = 0.001$

Figure 7: Phase portraits illustrating show a periodic behavior of system (19) for the chosen values of parameter I. Moreover, for each value of I, there is the same number of spikes within burst in time series and the same number of laps in the phase portraits

the onset of the step to the steady repetitive firing. Fig. 8a and 8b illustrates the periodic burst pattern with steady reptitive firing.

When $a = 1$, $b = 3$, $c = 1$, $d = 5$, $r = 0.005$, $s = 4$, $I = 3.25$, a deterministic system producing a burst with a random structure [40, 41] is generated. Fig. 8c and 8d illustrates periodic burst with random structure.

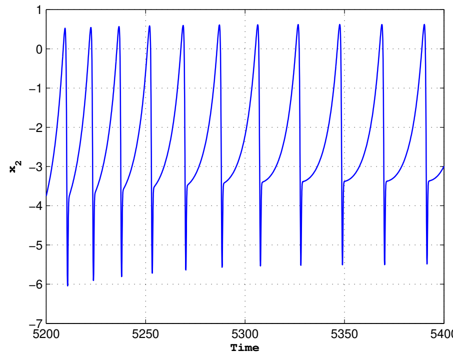

a) Time series portraits of the system (19) with parameters given in (20) with $I = 3$ for $r = 0.001$, a period doubling cascade with a period three solution is observed

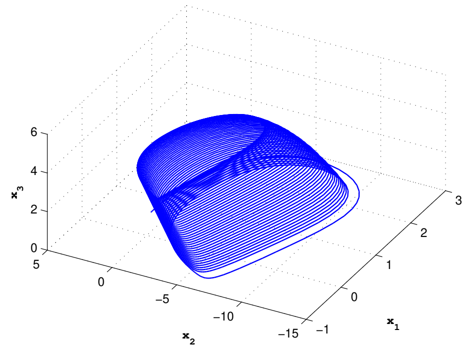

b) (x, y, z) phase portraits of the system (19) with parameters given in (20) with $I = 3$ for $r = 0.001$

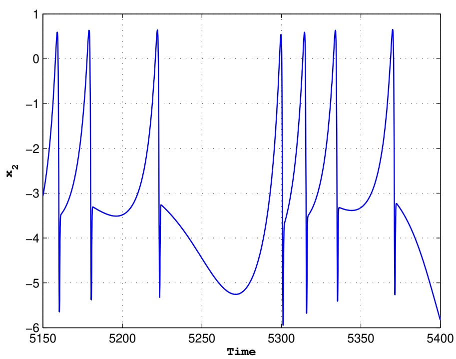

c) Time series portraits of the system (19) with parameters given in (20) with $I = 3.25$ for $r = 0.001$, the neuron behaviour changes from tonic spiking to bursting is observed

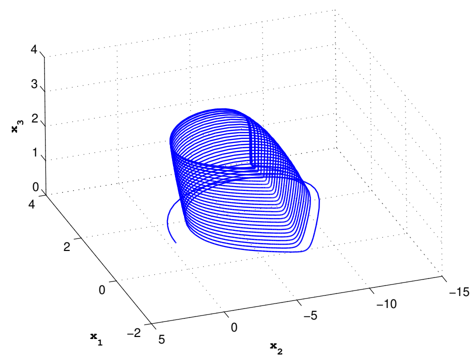

d) (x, y, z) phase portraits of the system (19) with parameters given in (20) with $I = 3.25$ for $r = 0.001$

Figure 8: Phase portraits illustrating show a periodic behavior of system (19) for the chosen values of parameter I and spikes and laps

4. Synchronization of neuronal model using backstepping control with recursive feedback

The plant system dynamics [48, 49] is described as

$$\begin{aligned} \dot{x}_1 &= x_2 - ax_1^3 + bx_1^2 - x_3 + I, \\ \dot{x}_2 &= c - dx_1^2 - x_2, \\ \dot{x}_3 &= r[s(x_1 - x_0) - x_3], \end{aligned} \tag{21}$$

where x_1, x_2, x_3 are state variables. a, b, c, d and x_0 are positive parameters of the neuronal impulsive system.

The observer system dynamic also defined as neuronal impulsive system [48, 49], and the system dynamics is described by

$$\begin{aligned} \dot{y}_1 &= y_2 - a y_1^3 + b y_1^2 - y_3 + I + u_1 , \\ \dot{y}_2 &= c - d y_1^2 - y_2 + u_2 , \qquad \dot{y}_3 = r[s(y_1 - y_0) - y_3] + u_3 , \end{aligned} \tag{22}$$

where $y_1,\ y_2,\ y_3$ are state variables.

Let the error be defined as

$$e_1 = y_1 - x_1 , \qquad e_2 = y_2 - x_2 , \qquad e_3 = y_3 - x_3 . \tag{23}$$

The error dynamics is obtained as

$$\begin{aligned} \dot{e}_1 &= e_2 - a(y_1^3 - x_1^3) + b e_1 (y_1 + x_1) - e_3 + u_1 , \\ \dot{e}_2 &= -d e_1 (y_1 + x_1) - e_2 + e_3 - y_3 + x_3 + u_2 , \qquad \dot{e}_3 = r s e_1 - r e_3 + u_3 . \end{aligned} \tag{24}$$

First consider the stability of the system

$$\dot{e}_1 = e_2 - a(y_1^3 - x_1^3) + b e_1 (y_1 + x_1) - e_3 + u_1 , \tag{25}$$

where e_2 regarded as virtual controller.

The Lyapunov function is defined by

$$V_1(e_1) = \frac{1}{2} e_1^2 , \tag{26}$$

and its derivative is as follows

$$\dot{V}_1 = e_1 \dot{e}_1 = e_1 \left(e_2 - a(y_1^3 - x_1^3) - e_3 + u_1 \right) . \tag{27}$$

Assume the controller $e_2 = \alpha_1(e_1)$. If

$$\begin{aligned} &\alpha_1(e_1) = -k_1 e_1 \\ &\text{and} \\ &u_1 = e_3 + a(y_1^3 - x_1^3) - b e_1 (y_1 + x_1), \end{aligned} \tag{28}$$

then

$$\dot{V}_1(e_1) = -k_1 e_1^2 \tag{29}$$

which is a negative definite function. Hence the system (25) is globally asymptotically stable.

The function $\alpha_1(e_1)$ is an estimative when e_2 is regarded as virtual controller.

The error between e_2 and $\alpha_1(e_1)$ is

$$w_2 = e_2 - \alpha_1(e_1) = e_2 + k_1 e_1 . \tag{30}$$

Consider (e_1, w_2) subsystem given by

$$\begin{aligned} \dot{e}_1 &= w_2 - k_1 e_1 , \\ \dot{w}_2 &= -de_1(y_1 + x_1) - (1 - k_1)(w_2 - k_1 e_1) + e_3 - y_3 + x_3 + u_2 . \end{aligned} \tag{31}$$

Let e_3 be a virtual controller in (30).

Assume that when $e_3 = \alpha_2(e_1, w_2)$, the system (30) is globally exponentially stable. Consider the Lyapunov function defined by

$$V_2(e_1, w_2) = V_1(e_1) + \frac{1}{2} w_2^2 . \tag{32}$$

The derivative of $V_2(e_1, w_2)$ is

$$\begin{aligned} \dot{V}_2(e_1, w_2) &= \dot{V}_1 + w_2 \dot{w}_2 , \\ \dot{V}_2(e_1, w_2) &= -k_1 e_1^2 + w_2(e_1 - de_1(y_1 + x_1) - (1 - k_1)(w_2 - k_1 e_1) \\ &\quad + e_3 - y_3 + x_3 + u_2 . \end{aligned} \tag{33}$$

Substituting for e_3 (30) into (32)

$$\begin{aligned} \dot{V}_2(e_1, w_2) &= -k_1 e_1^2 + w_2(e_1 - de_1(y_1 + x_1) - (1 - k_1)(w_2 - k_1 e_1) \\ &\quad + \alpha_2(e_1, w_2) - y_3 + x_3 + u_2 . \end{aligned} \tag{34}$$

If

$$\alpha_2(e_1, w_2) = -e_1 - k_2 w_2 + (1 - k_1)(w_2 - k_1 e_1)$$

and

$$u_2 = de_1(y_1 + x_1) + y_3 - x_3 , \tag{35}$$

then

$$\dot{V}_2(e_1, w_2) = -k_1 e_1^2 - k_2 w_2 \tag{36}$$

which is a negative definite function. Hence the system (30) is globally asymptotically stable.

The function $\alpha_2(e_1, w_2)$ is an estimative when e_3 is regarded as virtual controller.

The error between e_3 and $\alpha_2(e_1, w_2)$ is

$$w_3 = e_3 - \alpha_2(e_1, w_2) = e_3 + e_1 + (k_1 + k_2 - 1)w_2 + (1 - k_1)k_1 e_1 . \tag{37}$$

Consider (e_1, w_2, w_3) subsystem given by

$$\begin{aligned} \dot{e}_1 &= w_2 - k_1 e_1 , \\ \dot{w}_2 &= w_3 - e_1 - k_2 w_2 , \\ \dot{w}_3 &= rse_1 - re_3 + (w_2 - k_1 e_1)(1 + k_1 - k_1^2) \\ &\quad + (k_1 + k_2 - 1)(w_3 - e_1 - k_2 w_2) + u_3 . \end{aligned} \tag{38}$$

Consider the Lyapunov function

$$V_3(e_1, w_2, w_3) = V_2(e_1, w_2) + \frac{1}{2}w_3^2\,. \tag{39}$$

The derivative of $V_3(e_1, w_2, w_3)$ is

$$\dot{V}_3 = \dot{V}_2(e_1, w_2) + \dot{w}_3 w_3 \tag{40}$$

i.e.,

$$\begin{aligned}\dot{V}_3 = -k_1e_1^2 - k_2w_2^2 + w_3[w_2 + rse_1 - re_3 + (w_2 - k_1e_1)(1 + k_1 - k_1^2)\\ + (k_1 + k_2 - 1)(w_3 - e_1 - k_2w_2) + u_3].\end{aligned} \tag{41}$$

Choose the controller u_3 as follows

$$\begin{aligned}u_3 = -w_2 - rse_1 + re_3 - (1 + k_1 - k_1^2)(w_2 - k_1e_1)\\ - (k_1 + k_2 - 1)(w_3 - e_1 - k_2w_2) - k_3w_3\,.\end{aligned} \tag{42}$$

Substituting for u_3 form (41) into (40), which give

$$\dot{V}_3 = -k_1e_1^2 - k_2w_2^2 - k_3w_3^2 \tag{43}$$

which is negative definite function on R^3. Thus by Lyapunov stability theory [42], the error dynamics (23) is globally exponentially stable for all initial conditions $e_0 \in R^n$.

Hence, the states of plant and observer systems are globally exponentially synchronized.

5. Numerical simulation

For the numerical simulations, the fourth order Runge-Kutta method is used to solve the system of differential equations (20) and (21) with the backstepping controls u_1, u_2 and u_3 given by equations (27), (34) and (41). The parameters of the systems (20) and (21) are taken in the case as $a = 1$, $b = 3$, $c = 1$, $d = 5$, $r = 0.005$, $s = 4$ and $I = 3.25$. The initial values of the plant system are chosen as: $x_1 = 0.632$, $x_2 = 0.912$ and $x_3 = 0.125$.

The initial value of the observer system are chosen as: $y_1 = 1.245$, $y_2 = 0.123$ and $y_3 = 0.001$.

Fig. 9 depicts the synchronization of Hindmarsh-Rose neuronal bursting when the injected current in the neuron $I = 1,\ 1.5$ and the ratio of time scales between spiking(fast dynamics) and resting(slow dynamics) $r = 0.001$.

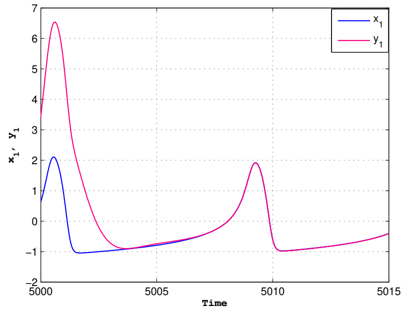

a) synchronization of membrane potential when the injected current in the neuron $I = 1$ and the ratio of time scales between spiking (fast dynamics) and resting (slow dynamics) $r = 0.001$

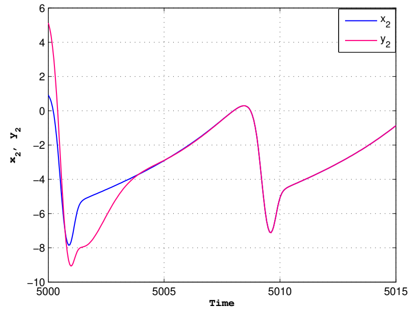

b) synchronization of electrode (the exchange of ions across the neuron membrane through fast ionic channels) when the injected current in the neuron $I = 1$ and the ratio of time scales between spiking(fast dynamics) and resting(slow dynamics) $r = 0.001$

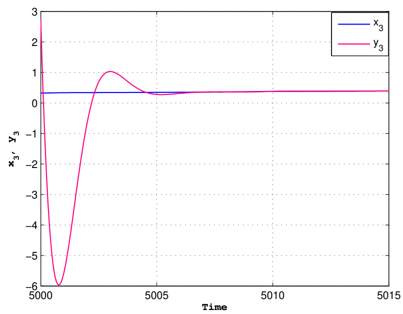

c) synchronization of intrinsic current(the exchange of ions through slow ionic channels) when the injected current in the neuron $I = 1$ and the ratio of time scales between spiking(fast dynamics) and resting(slow dynamics) $r = 0.001$

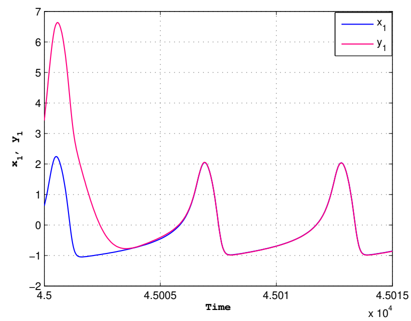

d) synchronization of membrane potential when the injected current in the neuron $I = 1.5$ and the ratio of time scales between spiking and resting $r = 0.001$

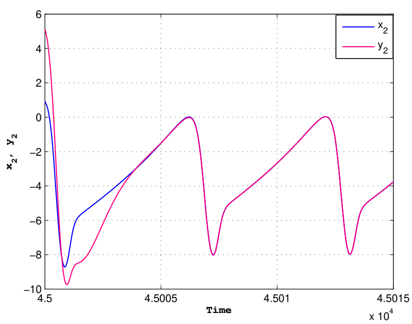

e) synchronization of the exchange of ions across the neuron membrane through fast ionic channels when the injected current in the neuron $I = 1.5$ and the ratio of time scales between spiking and resting $r = 0.001$

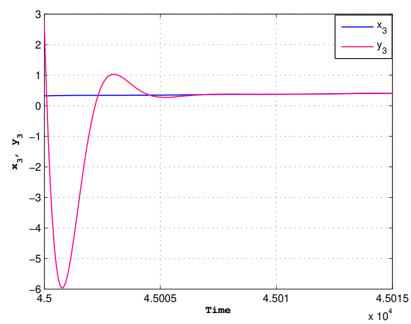

f) synchronization of the exchange of ions through slow ionic channels when the injected current in the neuron $I = 1.5$ and the ratio of time scales between spiking and resting $r = 0.001$

Figure 9: Phase portraits of synchronization

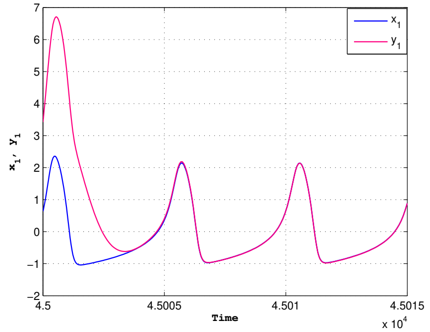

a) synchronization of membrane potential when the injected current in the neuron $I = 2$ and the ratio of time scales between spiking and resting $r = 0.001$

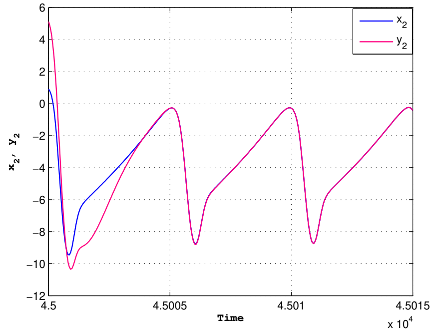

b) synchronization of the exchange of ions across the neuron membrane through fast ionic channels when the injected current in the neuron $I = 2$ and the ratio of time scales between spiking and resting $r = 0.001$

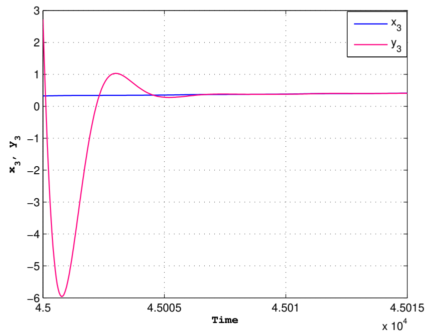

c) synchronization of the exchange of ions through slow ionic channels when the injected current in the neuron $I = 2$ and the ratio of time scales between spiking and resting $r = 0.001$

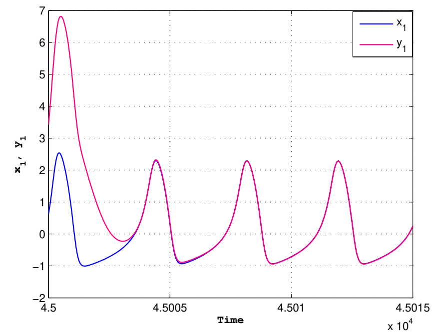

d) synchronization of membrane potential when the injected current in the neuron $I = 3$ and the ratio of time scales between spiking and resting $r = 0.001$

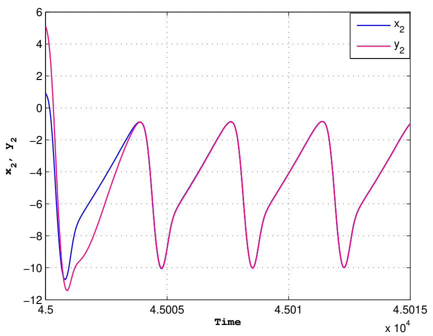

e) synchronization of the exchange of ions across the neuron membrane through fast ionic channels when the injected current in the neuron $I = 3$ and the ratio of time scales between spiking and resting $r = 0.001$

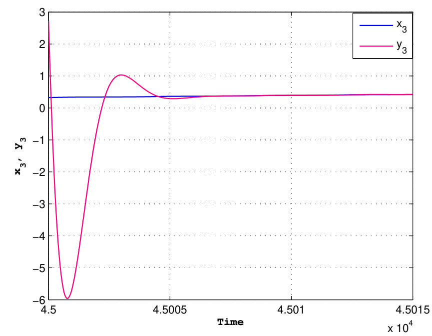

f) synchronization of the exchange of ions through slow ionic channels when the injected current in the neuron $I = 3$ and the ratio of time scales between spiking and resting $r = 0.001$

Figure 10: Phase portraits of synchronization

Fig. 10 depicts the synchronization of Hindmarsh-Rose neuronal bursting when the injected current in the neuron $I = 2,\ 3$ and the ratio of time scales between spiking(fast dynamics) and resting(slow dynamics) $r = 0.001$.

Fig. 11 depicts the synchronization of Hindmarsh-Rose neuronal bursting when the injected current in the neuron $I = 3.25$ and the ratio of time scales between spiking(fast dynamics) and resting(slow dynamics) $r = 0.001$.

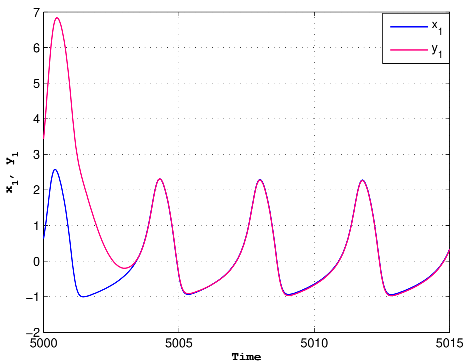

a) synchronization of membrane potential when the injected current in the neuron $I = 3.25$ and the ratio of time scales between spiking and resting $r = 0.001$

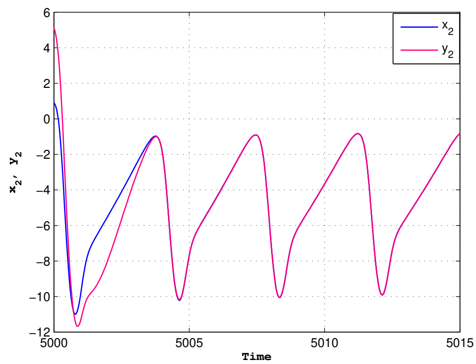

b) synchronization of the exchange of ions across the neuron membrane through fast ionic channels when the injected current in the neuron $I = 3.25$ and the ratio of time scales between spiking and resting $r = 0.001$

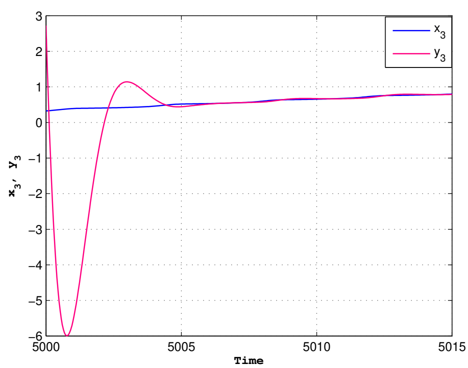

c) synchronization of the exchange of ions through slow ionic channels when the injected current in the neuron $I = 3.25$ and the ratio of time scales between spiking and resting $r = 0.001$

Figure 11: Phase portraits of synchronization

Fig. 12 depicts the synchronization of Hindmarsh-Rose neuronal bursting when the injected current in the neuron $I = 3.25$ and the ratio of time scales between spiking(fast dynamics) and resting(slow dynamics) $r = 0.0001$.

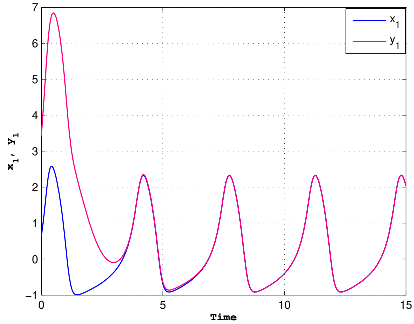

a) synchronization of membrane potential when the injected current in the neuron $I = 3.25$ and the ratio of time scales between spiking and resting $r = 0.0001$

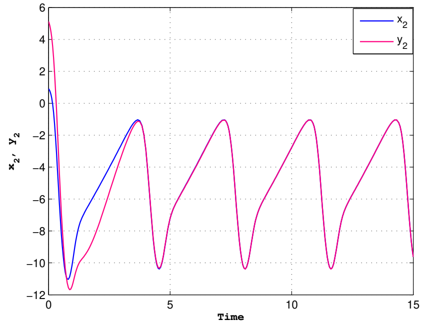

b) synchronization of the exchange of ions across the neuron membrane through fast ionic channels when the injected current in the neuron $I = 3.25$ and the ratio of time scales between spiking and resting $r = 0.0001$

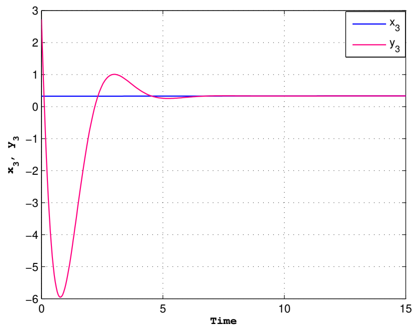

c) synchronization of the exchange of ions through slow ionic channels when the injected current in the neuron $I = 3.25$ and the ratio of time scales between spiking and resting $r = 0.0001$

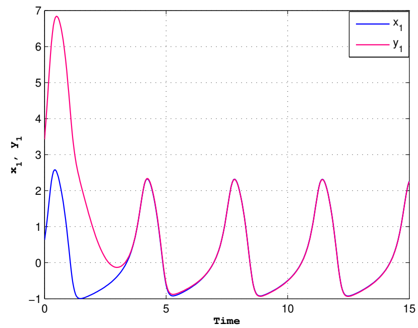

d) synchronization of membrane potential when the injected current in the neuron $I = 3.25$ and the ratio of time scales between spiking and resting $r = 0.0017$

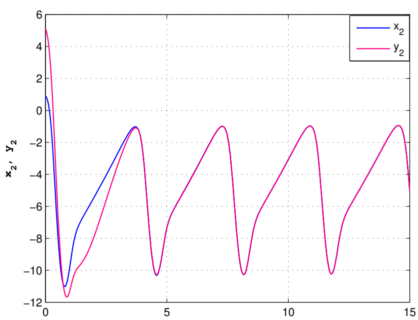

e) synchronization of the exchange of ions across the neuron membrane through fast ionic channels when the injected current in the neuron $I = 3.25$ and the ratio of time scales between spiking and resting $r = 0.0017$

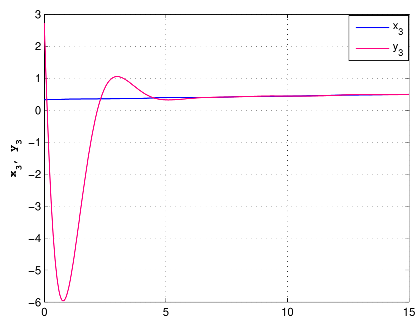

f) synchronization of the exchange of ions through slow ionic channels when the injected current in the neuron $I = 3.25$ and the ratio of time scales between spiking and resting $r = 0.0017$

Figure 12: Phase portraits of synchronization

6. Conclusion

In this paper, the backstepping control method has been applied to achieve global chaos synchronization for Hindmarsh-Rose neuronal bursting systems. Since the Lyapunov exponents are not required for these calculations, the backstepping control design is very effective and convenient to achieve global chaos synchronization. Numerical simulations have been given to illustrate and validate the effectiveness of the backstepping control based synchronization schemes of the neuronal systems.

References

[1] Qingkai Han, LinaHao, Hao Zhang and Bangchun Wen: Achivement of chaotic synchronization trajectrories of masterslave manipulators with feedback control strategy. *Acta Mech. Sin.*, **26** (2010), 433–439.

[2] G.M. Mahmoud, T. Bountis, G.M. AbdEI-Latif and E.E. Mahmoud: Chaos synchronization of two different chaotic complex Chen and Lu systems. *Nonlinear Dyn.*, **55** (2009), 43–53.

[3] Hamid Reza Karimi and Huijun Gao: LMI based H1 synchronization of second order neutral master-slave system using delayed output feedback control. *International Journal of Control, Automation and Systems*, **7** (2009), 371–380.

[4] Chaio-Shiung Chen and Heng-Hui Chen: Intelligent quadratic optimal synchronization of uncertain chaotic system via LMI approach. *Nonlinear Dyn.*, **63** (2011), 171–181.

[5] Wangli He and Jinde Cao: Exponential synchronization of chaotic neural networks: a matrix measure approach, *Nonlinear Dyn.*, **55** (2009), 55–65.

[6] Wu Xiao-qun and Lu Jun-an: Synchronization of unified chaotic system using occasional driving, Wuhan University *Wuhan Univ. J. of Nat. Sci.*, **8** (2003), 808–812.

[7] K. Murali and M. Lakshmanan: Secure communication using a compound signal using sampled-data feedback, *Applied Mathematics and Mechanics*, **11** (2003), 1309–1315.

[8] T. Yang and L.O. Chua: Generalized synchronization of chaos via linear transformations. *Internat. J. Bifur. Chaos*, Vol. **9** (1999), 215–219.

[9] K. Murali and M. Lakshmanan: *Chaos in Nonlinear Oscillators: Controlling and Synchronization*, Singapore: World Scientific (1996).

[10] S.K. Han, C. Kerrer and Y. Kuramoto: D-phasing and bursting in coupled neural oscillators. *Phys. Rev. Lett.*, **75** (1995), 3190–3193.

[11] B. Blasius, A. Huppert and L. Stone: Complex dynamics and phase synchronization in spatially extended ecological system. *Nature*, **399** (1999), 354–359.

[12] L. Kocarev and U. Parlitz: General approach for chaotic synchronization with applications to communications. *Phys. Rev. Lett.*, **74** (1995), 5028–5030.

[13] Zuolei Wang: Chaos synchronization of an energy resource system based on linear control. *Nonlinear Analysis: Real world Application*, **11**(5), (2010), 3336–3343.

[14] Jiang Wang, Lisong Chen and Bin Deng: Synchronization of ghostburster neurons in external electrical stimulation via H1 variable universe fuzzy adaptive control. *Chaos, Solitons and Fractals*, **39** (2009), 2076–2085.

[15] Moukam Kakmeni, F. M., Nguenang, J. P. and Kofane, T. C.: Chaos synchronization in bi-axial magnets modeled by bloch equation. *Chaos, Solitons and Fractals*, Vol. 30,pp. 690–699, (2006).

[16] J.L. Hindmarsh and R.M. Rose: A model of neuronal bursting using 3-coupled first order differential equations. *Proc. Roy. Soc. Lond. B. Biol*, **221** (1984), 81–102.

[17] Yan-Qiu Che, Jiang Wang, Kai-Ming Tsang and Wai-Lok Chen: Unidirectional synchronization for Hindmarsh-Rose neurons via robust adaptive sliding mode control. *Nonlinear Analysis: Real world Application*, **11** (2010), 1096–1104.

[18] Guang Zhao Zeng, Lan Sun Chen and Li Hua Sun: Complexity of an SIR epidemic dynamics model with impulsive vaccination control. *Chaos, Solitons and Fractals*, **26** (2005), 495–505.

[19] Junxa Wang, Dianchen Lu and Lixin Tian: Global synchronization for time delay WINDMI system. *Chaos, Solitons and Fractals*, **30** (2006), 629–635.

[20] Lin Pan, Wuneng, Jianan Fang and Dequan Li: A novel active pinning control for synchronization and antisynchronization of new uncertain unified chaotic systems. *Nonlinear Dyn.*, **62** (2010), 417–425.

[21] Xuerong Shi and Zuolei Wang: Robust chaos synchronization of four dimensional energy resource system via adaptive feedback control. *Nonlinear Dyn.*, **60**(4) (2010), 631–637.

[22] Quanxin Zhu and Jinde Cao: Adaptive synchronization of chaotic cohen-crossberg neural networks with mixed time delays. *Nonlinear Dyn.*, **61** (2010), 517–534.

[23] Jiakun Zhao and Tao Ren: Q-S synchronization between chaotic systems with double scalling functions. *Nonlinear Dyn.*, **62** (2010), 665–672.

[24] Haozhou Zheng, Jinfeng Hu, Peng Wu, Lidong Liu and Zishu He: Study on synchronization and parameters in sensitivity of a class of hyperchaotic systems using nonlinear feedback control. *Nonlinear Dyn.*, **67**(2) (2012), 1515–1523.

[25] S. Bowong and J.J. Tewa: Practical adaptive synchronization of a class of uncertain chaotic system. *Nonlinear Dyn.*, **56** (2009), 57–68.

[26] M.Arefi and M.R. Jahed-Motlogh: Robust synchronization of Rossler systems with mismatched time-varying parameters. *Nonlinear Dyn.*, **67**(2) (2012), 1233–1245.

[27] Choon Ki Ahn: Neural network H1 chaos synchronization. *Nonlinear Dyn.*, **60** (2010), 295–302.

[28] Wei-Sheng Chen, Rui-Hong Li and Jing Li: Observer-based adaptive iterative learning control for nonlinear systems with time varying delays. *Int. Journal of Automation and Computing*, **7** (2010), 438–446.

[29] H. Adloo, N. Noroozi and P. Karimaghaee: Observer-based model reference adaptive control for unknown time-delay chaotic systems with input nonlinearity. *Nonlinear Dyn.*, **67**(2) (2012), 1337–1356.

[30] Abdurahman Kadir, Xing-Yuan Wang and Yu-Zhang Zhao: Robust adaptive fuzzy neural tracking control for a class of unknown chaotic systems. *PRAMANA – Journal of Physics*, **76** (2011), 887–900.

[31] S. Bowong: Adaptive synchronization of chaotic systems with unknown bounded uncertainities via backstepping approach. *Nonlinear Dyn.*, **49** (2007), 59–70.

[32] Lu Ling, Li Yi and Guo ZhiAn: Parameter identification and synchronization of spatiotemporal chaos inan uncertain Gray-scott system. *Science in China Series G: Physics, Mechanics*, **51** (2008), 1638–1646.

[33] Jianxiong Zhang and Wanstieng Tang: Control and synchronization for a class of new chaotic systems via linear feedback. *Nonlinear Dyn.*, **58** (2009), 675–686.

[34] Zuo Lei Wang and Xue Rong Shi: Adaptive Q-S synchronization of non-identical chaotic systems with unknown parameters. *Nonlinear Dyn.*, **59** (2010), 559–567.

[35] Chi-Ching Yang: Adaptive synchronization of Lu hyperchaotic system with uncertain parameters based on single input controller. *Nonlinear Dyn.*, **63** (2010), 447–454.

[36] Di-Yi Chen, Lin Shi, Hai-Tao Chen and Xiao-Yi Ma: Analysis and control of a hyperchaotic system with only one nonlinear term. *Nonlinear Dyn.*, **67**(3) (2012), 1745–1752.

[37] Xiang-Jon Wu and Hong-Tao Lu: Generalized projective log synchronization between different hyperchaotic systems with uncertain parameters. *Nonlinear Dyn.*, **66**(1-2) (2011), 185–200.

[38] Chunali Mu, Fuchen Zhang, Yonglu Shu and Shouming Zhou: On the boundedness of solutions to the Lorenz-like family of chaotic systems. *Nonlinear Dyn.*, **67**(2) (2012), 987–996.

[39] V. Nenadovic, R. Whitney, J. Boulet and M.A. Cortez: Hypsarrhythmia in epileptic spasms: Synchrony in chaos. *Seizure*, **58** (2018), 55–61.

[40] L. Glass, M.R. Guevara and A. Shrier: Bifurcation and chaos in a periodically stimulated cardiac oscillator. *Physica 7D* (1983), 89–101.

[41] M.A. Quiroz-Juarez, R. Vazquez-Medina, E. Ryzhii, M. Ryzhii and J.L. Aragon: Quasiperiodicity route to chaos in cardiac conduction model. *Commun. Nonlinear Sci. Numer. Simulat.*, **42** (2017), 370–378.

[42] Somayeh Raiesdana and S. MohammadHashemi Goplayegani: Study on chaos anti-control for hippocampal models of epilepsy. *Neurocomputing*, **111** (2013), 54–69.

[43] F.M. de Paula Neto, W.R. de Oliveira, T.B. Ludermir and A.J. da Silva: Chaos in a quantum neuron: an open system approach. *Neurocomputing* (2017), doi: 10.1016/j.neucom.2016.06.081.

[44] U.E. Kocamaz, H. Tapkyn, Y. Uyaroolu and A. Goksu: Control and Synchronization of Chaotic Supply Chains using Intelligent Approaches. Computers & Industrial Engineering (2016), doi: http://dx.doi.org/10.1016/j.cie.2016.03.014.

[45] Quan Zhou, Wei Zhang, Scott Cash, Oluremi Olatunbosun, Hongming Xu and Guoxiang Lu: Intelligent sizing of a series hybrid electric power-train system based on Chaos-enhanced accelerated particle swarm optimization. *Applied Energy*, **189** (2017), 588–601.

[46] Yimin Yang, Yaonan Wang, Xiaofang Yuan and Feng Yin: Hybrid chaos optimization algorithm with artificial emotion. *Applied Mathematics and Computation*, **218** (2012), 6585–6611.

[47] U.E. Vincent, R.K. Odunaike, J.A. Laoye and A.A. Gbindinniuola: Adaptive backstepping control and synchronization of a modified and chaotic van der pol duffing oscillatror. *Journal Control Theory Application*, **9** (2011), 273–271.

[48] J.L. Hindmarsh and R.M. Rose: A model of the nerve impulse using two first order differential equations. *Nature*, **296** (1982), 162–164.

[49] J.L. Hindmarsh and R.M. Rose: A model of neuronal bursting using three coupled first order differential equations. *Proceeding of the Royal Society B*, **221** (1984), 87–102.

[50] W. Hahn: *The Stability of Motion*. Berlin, Germany: Springer-Verlag, 1967.